Avant-projet pour la conception d'une combinaison sensible pour robot de la famille HRP

Laurent Blanchet
encadré par
Martin Battaglia et Abderrahmane Kheddar

1er Septembre 2009

Table des matières

Première partie
Présentation

1 Présentation du laboratoire

Le laboratoire où j'ai effectué ces travaux est une unité de recherche mixte internationale entre le Centre National de la Recherche Scientifique (CNRS), français, et le National Institute of Advanced Industrial Science and Technologie (AIST), sise à Tsukuba, Japon (cf annexe A). Cette unité mixte (UMI3218) est le laboartoire Franco-Japonais de robotique et opère à l'identique que les unités mixtes de recherche du CNRS (UMR) au niveau national, sauf que l'unité se fait avec un organisme étranger.

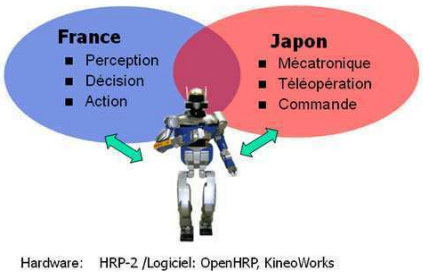

FIGURE 1 – Répartition des recherches.

Ce laboratoire a d'abord été une association sous forme d'un laboratoire international associé ; il a été initié par Dr. Philippe Coiffet (CNRS) et Prof. Kazuo Tanie (AIST) fin 2003, ce laboratoire conjoint poursuit l'accroissement de l'autonomie des robots, plus particulièrement au travers de travaux conduits sur les robots humanoïdes, qui constituent le support commun des recherches conduites par le JRL.

Le JRL est hébergé par l'Intelligent Systems Research Institute (cf annexe B), dont il fait partie. Parmi les sujets d'étude au JRL, nous nous intéressons à deux d'entre eux : la conception d'une semelle pour le robot HRP-2 dans le but de diminuer les vibrations induites soit par les impacts (création d'un contact et donc propagation de l'impact dans la structure polyarticulée) soit la rupture d'un contact lorsque les forces internes ne sont pas bien ajustées (le phénomène n'est pas régulier et a pour conséquence le même effet que la création d'un contact) ; et à la conception en avant-projet d'une combinaison sensible pour un bras.

2 Présentation du travail effectué

J'ai travaillé sur deux axes pendant ce stage : sur des éléments de la conception de la semelle et sur la création d'une combinaison haptique[1].

Je développe ma contribution dans les deux parties suivantes.

1. donnant le sens du toucher, même si ici on ne détecte que les efforts.

Deuxième partie

Conception de la combinaison haptique

3 Objet de l'avant-projet de combinaison

Figure 2 – HRP-4 et HRP-2.

Le travail effectué par le JRL, notamment Adrien Escande pour sa thèse, comprend un développement d'algorithmes permettant d'inclure dans la gestion de l'équilibre d'un robot des points d'appuis autre que ses jambes[6]. L'idée est de permettre au robot de s'assoir ou de prendre appui sur sa main ou son coude comme le ferait un humain (notamment dans le cadre du projet CWE[7]). Le problème qui s'est alors posé est l'absence de capteurs d'efforts permettant de localiser l'appui et de caractériser l'effort : le but de cette combinaison est donc de combiner une détection haptique avec une interaction sûre, le tout à faible coût.
La conception de la combinaison est divisée en trois couches :

- une peau constitué d'un élastomère,
- une matrice flexible tactile composé de capteurs tout-ou-rien,
- une carapace haptique[8] matérialisée par une coque solide assortie de capteurs sur sa face interne, que l'on va appeler macro-capteurs par opposition aux précédents.

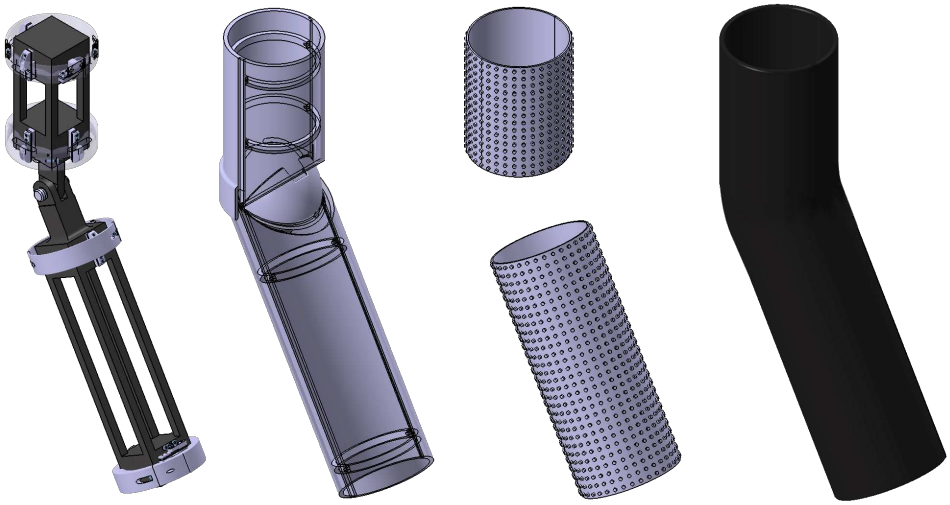

Figure 3 – Le squelette et les trois couches du bras.

6. Planification de points d'appuis pour la génération de mouvements acycliques : application aux humanoïdes. Thèse de doctorat, Université d'Evry-Val-d'Essonne, 2008.
7. Collaborative Work Environnement, voir aussi www.robot-at-cwe.eu.
8. relatif au sens du toucher. Ici on ne l'emploie que dans le sens que la carapace doit être sensible aux efforts.

Ces derniers assurent la liaison avec le squelette, qui est en fait la structure de base du robot. La peau doit permettre d'absorber le choc, la matrice tactile de localiser l'effort, et la carapace de caractériser le torseur de l'effort.

Martin Battaglia a précédemment mis en place des outils permettant de dimensionner la matrice flexible et posant des conditions sur la peau, avant de valider le principe avec un prototype d'un bras à un degré de liberté[9]. J'ai donc conçu la partie restante, c'est à dire la partie carapace haptique et sa liaison au squelette ainsi que la détermination de l'épaisseur de la peau.

4 Conception d'avant projet de la carapace haptique

4.1 Cahier des charges

Cette étude étant un avant-projet et se voulant général à la famille des HRP-xy, on prend pour le squelette une forme basique :

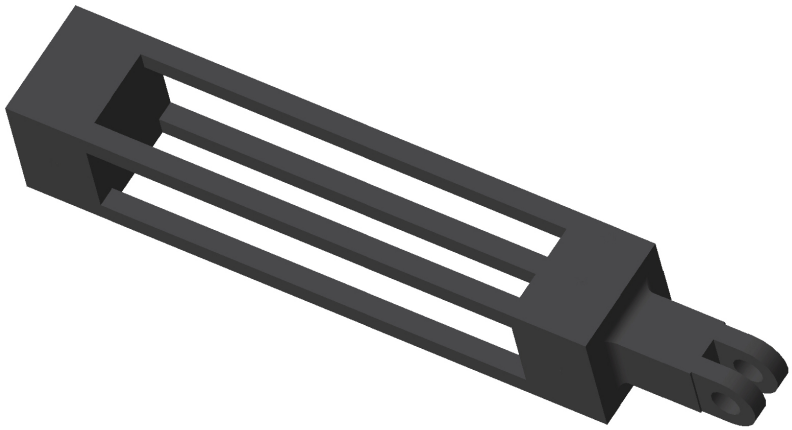

Figure 4 – Modèle utilisé comme squelette.

On a des contraintes fortes sur la conception de la liaison squelette-carapace et de la carapace haptique en elle-même :

- la liaison squelette - carapace doit permettre la mesure des six composantes du torseur des efforts extérieurs,
- compacité,
- légèreté,
- les zones utilisables du squelette se limitent aux blocs des deux extrémités,
- l'espace utilisé par la liaison et les macro-capteurs doit majoritairement être situé dans ces zones extrêmes et laisser l'espace libre au centre pour l'électronique, câbles, etc,
- être entièrement démontables et autoriser le remplacement du moindre élément sans que cela implique d'autres remplacements,
- être montables sur les robots comme un équipement (malgré les éventuelles articulations et solides aux extrémités du squelette),
- coût.

9. IROS 2009 (cf annexe G)

4.2 Détermination du torseur mesuré

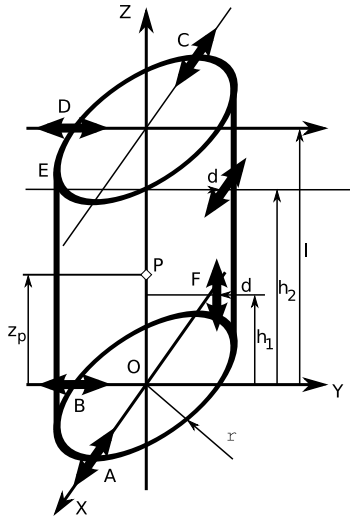

FIGURE 5 – Modèle de calcul.

La forme du torseur mesuré dépend du nombre de capteurs utilisés, soit ici 6 utilisés de manière bilatérale ou 12 unilatéralement. Comme la solution retenue n'utilise que 6 capteurs je présente le calcul correspondant. Je place deux capteurs par extrémité pour la mesures des efforts et moments des axes $\underline{x}$ et $\underline{y}$. Les capteurs pour l'effort selon $\underline{z}$ et le moment autour de cet axe vont être plus difficiles à implanter, je leur laisse donc plus de libertés de positionnement. Ainsi on a :

$$T_A = \left\{ \begin{array}{c|c} F_A & 0 \\ 0 & 0 \\ 0 & 0 \end{array} \right\}_{\begin{array}{l} r \\ 0 \\ 0 \end{array}} \qquad T_B = \left\{ \begin{array}{c|c} 0 & 0 \\ F_B & 0 \\ 0 & 0 \end{array} \right\}_{\begin{array}{l} 0 \\ -r \\ 0 \end{array}}$$

$$T_C = \left\{ \begin{array}{c|c} F_C & 0 \\ 0 & 0 \\ 0 & 0 \end{array} \right\}_{\begin{array}{l} -r \\ 0 \\ 0 \end{array}} \qquad T_D = \left\{ \begin{array}{c|c} 0 & 0 \\ F_D & 0 \\ 0 & 0 \end{array} \right\}_{\begin{array}{l} 0 \\ -r \\ 0 \end{array}}$$

$$T_E = \left\{ \begin{array}{c|c} F_E & 0 \\ 0 & 0 \\ 0 & 0 \end{array} \right\}_{\begin{array}{l} 0 \\ d \\ h_2 \end{array}} \qquad T_F = \left\{ \begin{array}{c|c} 0 & 0 \\ 0 & 0 \\ F_I & 0 \end{array} \right\}_{\begin{array}{l} 0 \\ d \\ h_1 \end{array}}$$

On peut calculer le torseur des efforts extérieurs, T_{ext} en un point de l'axe en supposant que le point d'application sur le derme est connu (rôle de la matrice tactile). Je prend donc T_{ext} en un point P de l'axe. Je ramène tous les torseurs des macro-capteurs au point P sur l'axe où je les somme :

$$T_{capteurs} = \left\{ \begin{array}{ll|l} F_A + F_C + F_E & & z_P \cdot F_B - (l - z_P) \cdot F_D + d \cdot F_F \\ F_B + F_D & & z_P \cdot F_A - (l - z_P) \cdot F_C + (h_2 - z_P) \cdot F_E \\ F_F & & -d \cdot F_E \end{array} \right\}_{\begin{array}{l} 0 \\ 0 \\ z_P \end{array}}$$

On voit bien que ce positionnement permet de mesurer toutes les composantes d'un effort extérieur quelconque.

4.3 Capteurs

Plusieurs solutions ont été envisagées, par ordre chronologique :

- capteurs de déplacement : utiliser un système de ressort pour déduire l'effort appliqué. Le problème était l'amplitude de déplacement, auquel on répond en adjoignant un système à 2 vérins (le premier à faible course et gros diamètre, le second à grande course et faible diamètre). Abandonné à cause du fluide qui nécessite une maintenance, de l'encombrement et de la complexité. (cf fig 6)

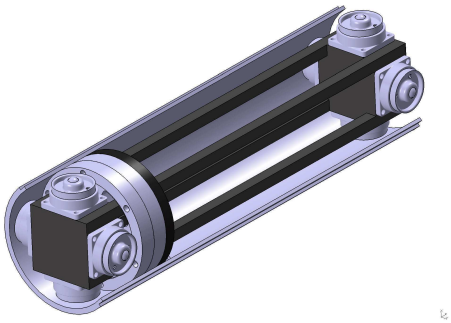

FIGURE 6 – 1ère architecture envisagée.

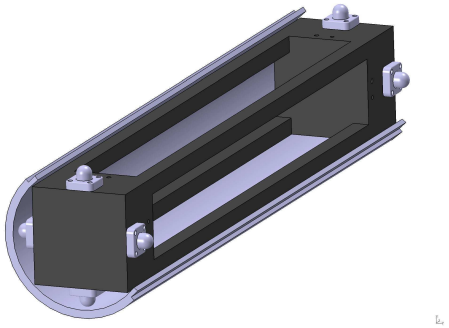

FIGURE 7 – 2nde architecture envisagée.

- capteurs d'efforts FlexiForce® : même architecture "vérin" que précédemment pour que l'effort soit appliqué sur toute la surface du capteur ; grande compacité, faible coût, mais performances faibles. (cf annexe C et fig 7)
- capteurs d'efforts Futek® FBB300 : un peu moins compacts, plus coûteux mais avec des performances satisfaisantes. Du fait du prix on désire en utiliser le minimum possible : 6. (cf annexe D et fig 8)

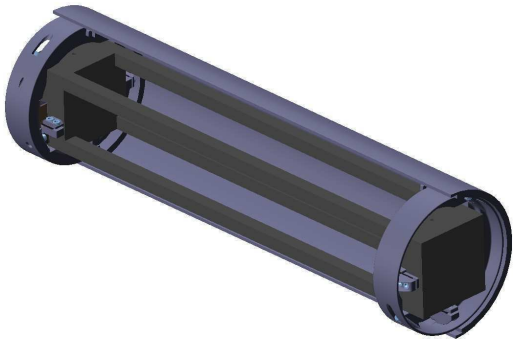

FIGURE 8 – Dernière architecture envisagée.

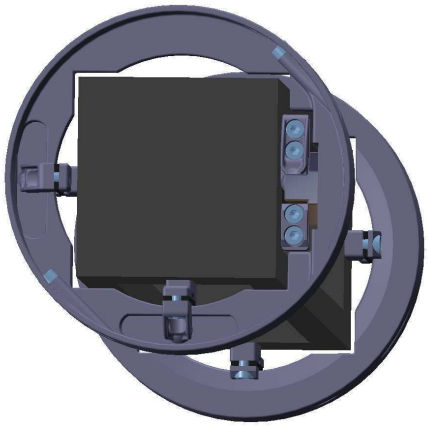

FIGURE 9 – Les capteurs des axes radiaux : sur le premier anneau, à gauche et en bas, sur le second à droite et en bas.

À cause de la contrainte de mesurer l'ensemble des composantes du torseur des actions extérieures et de la difficulté d'instrumenter suffisamment une liaison classique type "deux demi-rotules", "centrage court + appui-plan" ou "centrage long + ponctuelle", on se voit dans l'obligation de recourir à des solutions moins conventionnelles. Avec l'intention de mesurer toutes les composantes du torseur on aboutit à la conclusion que ce sont les capteurs qui vont réaliser la liaison par le biais de ponctuelles.

Pour les deux premières architectures on a donc choisi d'intercaler une bille entre la partie "piston" et la coque. Pour la troisième en revanche, pour réduire la dépense en capteurs, on doit réaliser des ponctuelles bilatérales au lieu de ponctuelles simples.

Pour les capteurs des axes $\underline{x}$ et $\underline{y}$, on utilise une cavité dans un anneau en PVC pour obtenir la bilinéarité, fig 9.

Pour les capteurs de l'effort et du moment sur $\underline{z}$, la petite taille de la pièce transmettant les efforts nécessite de la faire en aluminium au moins. Ainsi on obtient le capteur de l'effort selon

$\underline{z}$ fig 10 et le capteur du moment selon $\underline{z}$ fig 11.

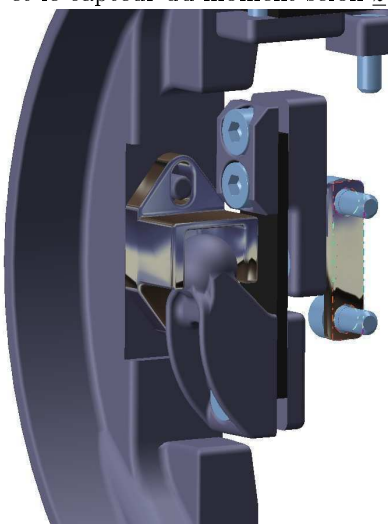

FIGURE 10 – Détail de l'implémentation du capteur d'effort sur z.

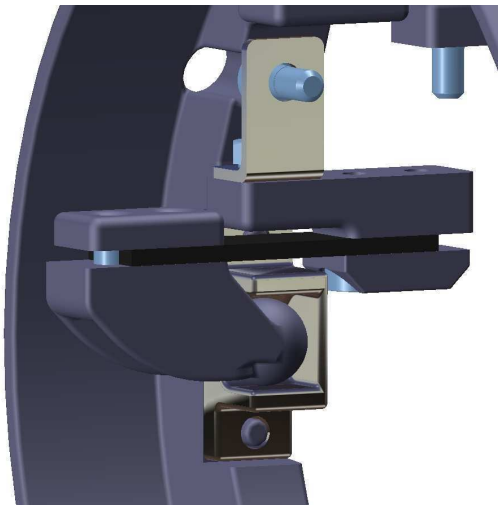

FIGURE 11 – Détail d'implémentation du capteur d'effort pour mesurer le moment sur z.

À part ces quatre pièces en aluminium, le reste peut-être fait en ABS ou en PVC. La complexité des formes de la poutre transmettant les efforts aux capteurs en particulier et la très petite série (prototype) tendent à orienter vers de l'impression 3D. L'injection plastique n'est pas exclue pour autant quand on considère la surface à couvrir (le robot entier).

On doit également protéger et instrumenter les articulations. On réduit le coût en capteur en réalisant l'extérieur de l'articulation par le biais des carapaces et l'intérieur par le biais d'une pièce en liaison pivot sur la carapace fig 12 :

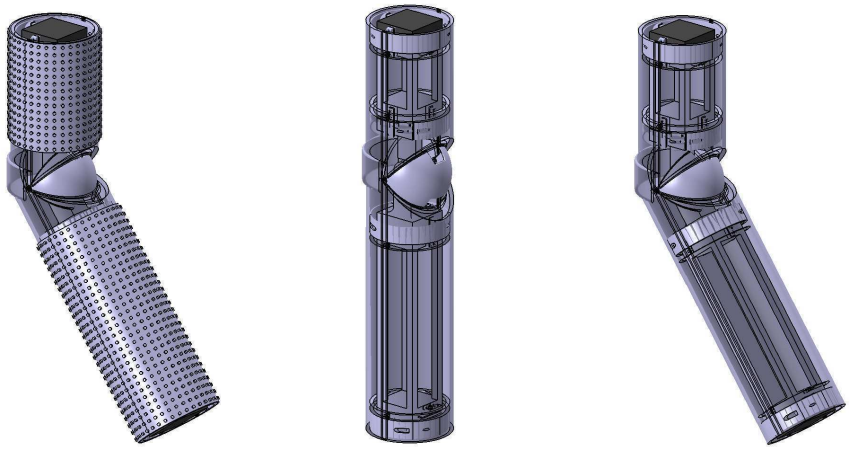

FIGURE 12 – Avec et sans la matrice tactile (représentation).

5 Dimensionnement de l'épaisseur de l'épiderme

On cherche une relation simple permettant de caractériser l'épaisseur minimale de l'épiderme. Le matériau choisi est une mousse de polyuréthane douce (St Gobain Korel ©K30-15, cf annexe E).

Les données sont : les caractéristiques matériau données par le constructeur, la masse du bras, la vitesse d'impact et la géométrie des deux solides, ainsi que divers résultats obtenus par Martin Battaglia, dont la durée de la compression jusqu'à la déformation maximale t_0. On se place dans le cas le plus défavorable, $m = 2\,kg \quad v = 1.5\,m.s^{-1}$ avec un obstacle de petite taille (sphère de $1\,cm$ de diamètre) et rigide ($E \to \infty$).

Une première approche serait de considérer un élément 1D soumis à une sollicitation de traction compression obéissant à la loi de Hooke $\sigma = E \cdot \varepsilon$.

Une seconde approche, celle-ci beaucoup plus réaliste, serait d'utiliser la théorie des plaques minces de Love-Kirchhoff ou la mécanique des milieux continus. L'ennui est que la solution au problème ne pourra être obtenue que par éléments finis au cas par cas et ne permettra pas d'obtenir une relation simple approchée.

Une troisième approche, énergétique, est retenue et consiste à considérer la résilience du matériau U_r qui définit l'énergie de déformation du matériau par unité de volume.

5.1 Approximation du volume absorbant le choc

On connait la surface du contact définie par les formules de Hertz[10] : on a un contact sphère/cylindre, aussi cette surface est elliptique et on note les demi-axes a et b.

On cherche à connaître la zone du tube qui se déforme au contact et donc qui absorbe l'impact. Les équations de la mécanique des milieux continus, malgré des simplifications importantes ne mènent à aucune solution analytique. On réalise donc une simulation en éléments finis (fig 13 & 14) à but purement qualitatif.

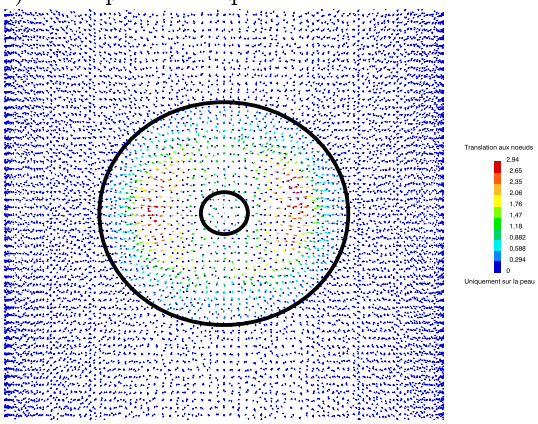

FIGURE 13 – Champ de déplacement du tube soumis à l'impact.

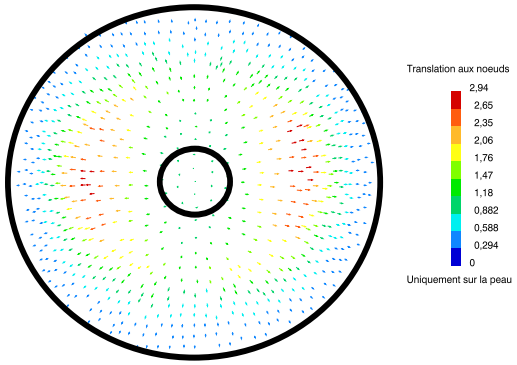

FIGURE 14 – Le même champ sans les déplacements nuls pour plus de lisibilité.

La première ellipse correspond à la zone de contact, la seconde délimite les déplacements non-nuls. Ce champ de déplacement a été obtenu pour une épaisseur de $5\,mm$, on obtient des résultats similaires pour $10\,mm$ et $15\,mm$. Au vu de la faible épaisseur de la peau et des résultats

10. http://www.digizeitschriften.de/index.php?id=loader&tx_jkDigiTools_pi1[IDDOC]=503750

des simulations, on va considérer que le volume du matériau qui absorbe le choc est le cylindre de même épaisseur que celle de l'épiderme e et de base la surface elliptique définie par quatre fois les demis-axes de la surface de contact, soit seize fois S_c.

5.2 Détermination de la surface de contact

5.2.1 Surface elliptique

On applique les formules de Hertz au contact cylindre/sphère pour obtenir la longueur des demis-axes de l'ellipse de la zone de contact :

$$\frac{1}{R_*} = \Sigma\rho = \frac{2}{r} + \frac{1}{R} \qquad f(\rho) = \sqrt{\frac{1}{R^2}} \qquad F(\rho) = \frac{f(\rho)}{\Sigma\rho}$$

d'où :

$$a = e_a \cdot \left(\frac{11550 \cdot F \cdot R_*}{E_*}\right)^{1/3} \qquad b = e_b \cdot \left(\frac{11550 \cdot F \cdot R_*}{E_*}\right)^{1/3}$$

On détermine les valeurs de e_a et e_b par interpolation du tableau annexe C.

$$\text{On a donc : } S_c = \pi \cdot e_a \cdot e_b \cdot \left(\frac{11550 \cdot F \cdot R_*}{E_*}\right)^{2/3}$$

Pour notre problème on a $E_* = \dfrac{E_{compression}}{1-\nu^2} = 82800\,Pa$, $f(\rho) = 20$, $F(\rho) = 0.091$, $R_* \approx 4.5\,mm$, $e_a = 0.0556$, $e_b = 0.0463$, soit : $S_c \approx 697\,mm^2$.

5.2.2 Approximation par une surface circulaire

Si on approxime la surface elliptique de contact définie par Hertz par une surface circulaire, dans le but de ne pas avoir à calculer e_a et e_b et de pouvoir simplement appliquer une formule donnant e, et comme $e_a \cdot e_b \cdot 11550^{2/3} \geq 1.3$, on peut simplement prendre :

$$S_c = 1.3 \cdot \pi \cdot \left(\frac{F \cdot R_*}{E_*}\right)^{2/3}$$

En minorant cette constante par 1.3, on va obtenir une épaisseur supérieure à la valeur obtenue sans l'approximation, ce qui ne pose pas de problème puisse qu'on cherche une valeur minimale de e.

Pour notre problème cette formule donne : $S_c \approx 690\,mm^2$.

5.3 Relation énergétique

La résilience U_r en compression est définie par : $U_r = \dfrac{\sigma^2_{yield\,in\,compression}}{2 \cdot E_{compression}}$.

Dès que le choc est détecté, le bras inverse son mouvement. Appelons la durée entre le contact jusqu'à ce que le bras commence le mouvement inverse t_0. L'énergie cinétique est appelée E_k.

Si on avait laissé l'impact aller à son terme, on aurait obtenu une indentation δ_c au bout du temps t_c et le bras aurait absorbé l'énergie cinétique E_k de l'impact. Cette durée t_c est donnée

par Martin Battaglia[11]. On suppose que le transfert d'énergie est linéaire par rapport au temps, aussi l'énergie transmise au bras devient $E_n = E_k \cdot (t_0/t_c)$.

Ici on a : $t_0 = 6\,ms$, $t_c = 32\,ms$ d'où $E_n = \frac{1}{2} \cdot m \cdot v^2 \cdot \frac{t_0}{t_c} = \frac{1}{2} \cdot 2 \cdot 1.5^2 \cdot \frac{6}{32} = 0,42\,J$

On définit le travail effectué par l'effort de contact W et on considère aussi que l'énergie cinétique est entièrement transmise au matériau (cas défavorable), $W = E_n$. En considérant que le volume qui absorbe l'énergie est le cylindre d'épaisseur e et de base $16S_c$ on a : $U_r \cdot e \cdot 16 \cdot S_c = E_n$.

5.4 Effort au contact

Pour évaluer l'effort au contact, on considère le travail effectué par cet effort pour déformer élastiquement la zone de contact : $W = F \cdot \delta_c$.

Or la théorie de Hertz nous donne aussi : (cf *Impact Mechanics, §6*)

$$\frac{W}{E_* \cdot R_*^3} = \frac{8}{15} \cdot \left(\frac{\delta_c}{R_*}\right)^{5/2} \qquad \text{D'où : } F = \left(\left(\frac{8}{15}\right)^2 \cdot E_k^3 \cdot E_*^2 \cdot R_*\right)^{1/5} \approx 40\,N$$

5.5 Épaisseur de la peau

L'épaisseur de la peau est finalement obtenue avec : $e = \dfrac{E_n}{U_r \cdot 16 S_c}$.

5.5.1 Surface ellipsoïde

Si on veut une approximation plus juste, on garde l'excentricité de la surface de contact : $e = E_n \cdot \left(U_r \cdot \pi \cdot 4e_a \cdot 4e_b \cdot \left(11550 \cdot R_* \cdot F \cdot E_*^{-1}\right)^{2/3}\right)^{-1}$

$$\text{D'où : } e = \frac{m^{3/5} \cdot v^{6/5} \cdot \dfrac{t_0}{t_c}}{U_r \cdot 655 \cdot 16\pi \cdot e_a \cdot e_b \cdot \left(R_*^2 \cdot E_*^{-1}\right)^{6/15}}$$

Pour notre problème : $e = 7.90\,mm$.

5.5.2 Approximation

Sans chercher à calculer e_a et e_b, on utilise l'approximation : $e = E_n \cdot \left(16 U_r 1.3\pi \left(R_* \cdot F \cdot E_*^{-1}\right)^{2/3}\right)^{-1}$

$$\text{D'où : } e = \frac{m^{3/5} \cdot v^{6/5} \cdot \dfrac{t_0}{t_c}}{84 \cdot U_r \cdot \left(R_*^2 \cdot E_*^{-1}\right)^{6/15}}$$

Pour notre problème : $e = 7.96\,mm$.

La différence n'est pas grande, mais c'est dû aux faibles dimensions de l'objet étranger qui conduit à une excentricité de la surface de contact faible.

11. IROS 2009 (cf annexe G)

Troisième partie
Conclusion

6 Perspectives

Dans un avenir proche, il est prévu de reconcevoir la combinaison pour l'adapter au squelette réel avec une structure 3D complexe et non poutre, puis de passer à la réalisation. Cela permettra de détecter les collisions, et de conserver l'intégrité du robot et de l'objet heurté (par exemple, une personne). De plus il permettra dans un futur proche au robot d'utiliser des appuis autre que ses pieds.

A Organisation AIST

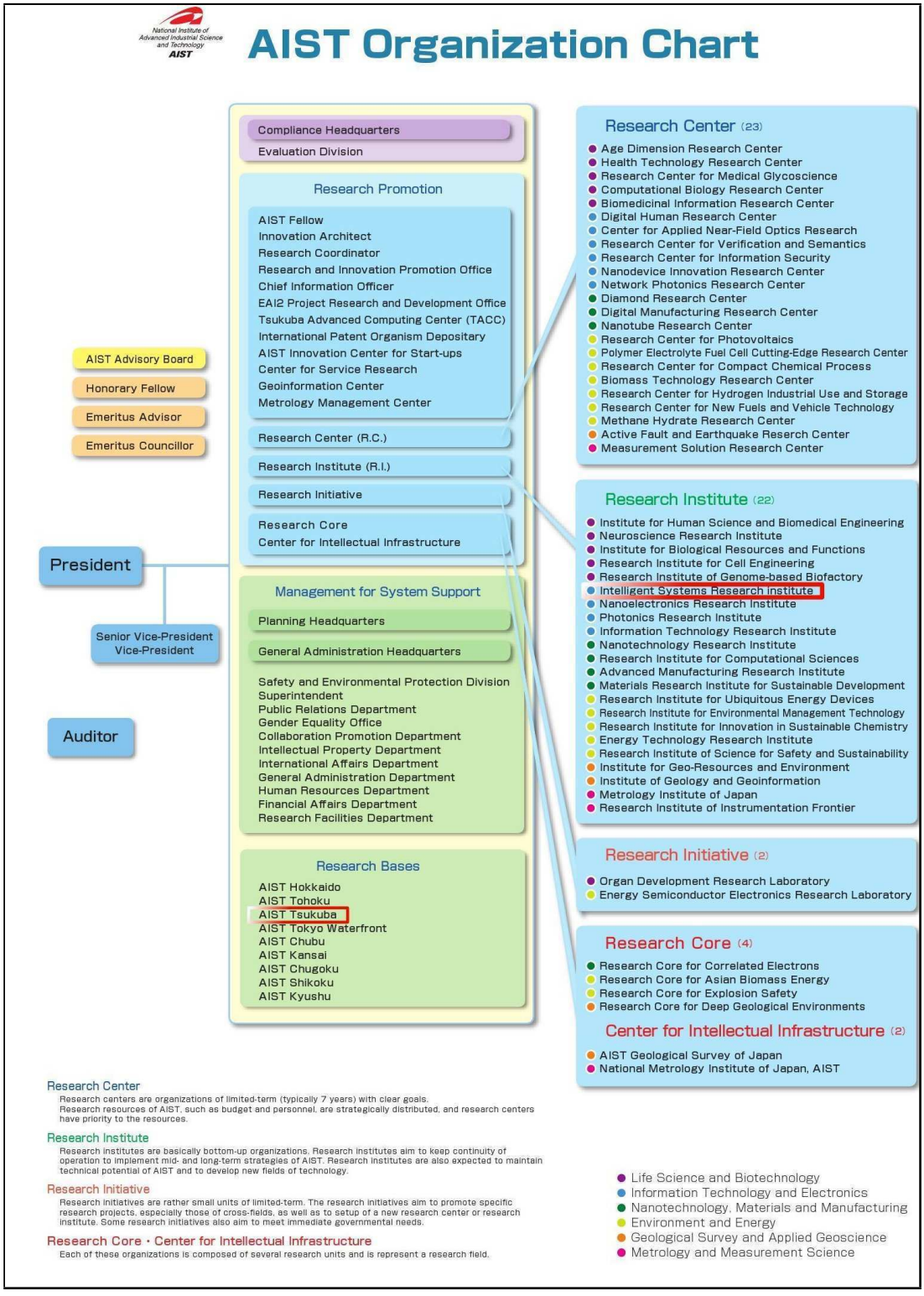

B Organisation ISRI

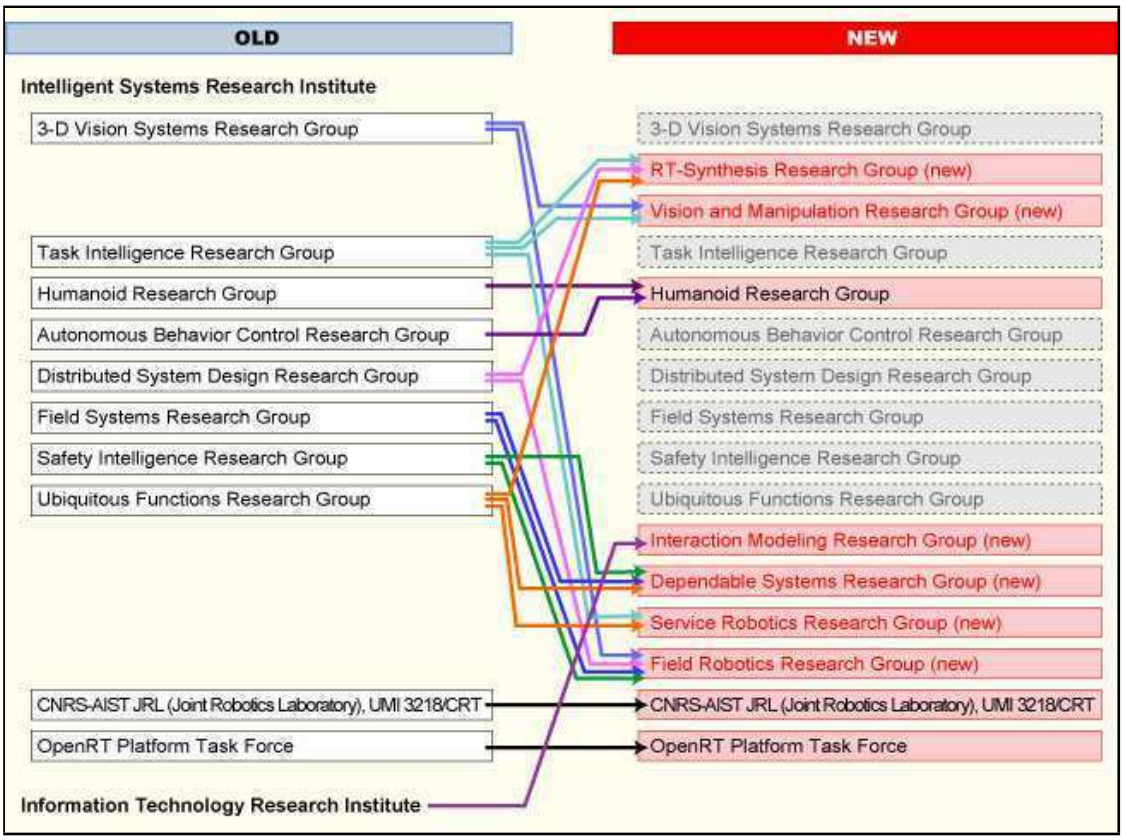

C Capteurs Flexiforce

Actual size of sensor

Physical Properties

Thickness	0.008” (0.203 mm)
Length	7.75” (197 mm)
optional	6” (152 mm)
trimmed	4” (102 mm)
lengths	2” (51 mm)
Width	0.55” (14 mm)
Sensing Area	0.375” (9.53 mm) diameter
Connector	3-pin Male Square Pin (center pin is inactive)
Substrate	Polyimide (ex: Kapton)

Available Force Ranges* (as tested with circuit shown)

HT201-L	Low: 0-30lb (0-133N)
HT201-H	High: 0-100lb (0-445N)

*In order to measure forces outside of specified ranges, use recommended circuit and adjust drive voltage and/or reference resistance.

Recommended Circuit

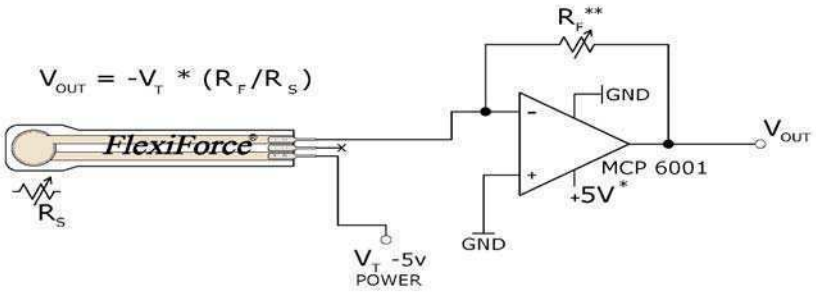

- * Supply Voltages should be constant
- ** Reference Resistance R_F is 1kΩ to 100kΩ
- Sensor Resistance R_S at no load is >5MΩ
- Max recommended current is 2.5mA

Typical Performance**

Linearity	±1.2% of full scale
Repeatability	±3.5% of full scale
Hysteresis	3.6% of full scale
Drift	3.3% per log time
Temperature Range	15°F to 400°F (-9°C to 204°C)
Output Change/Degree F	0.16%

**Specifications based on pressures up to 500 psi and represent the average value throughout a range of temperatures up to 400°F

FUTEK MODEL FBB300

PLANAR BEAM FORCE SENSOR (OEM)

(Previously FR1010)

Drawing Number: FI1113-B	
INCH [mm]	R.O.= Rated Output

WIRING CODE (WC1)			
+Excitation	-Excitation	+Signal	-Signal
RED	BLACK	GREEN	WHITE

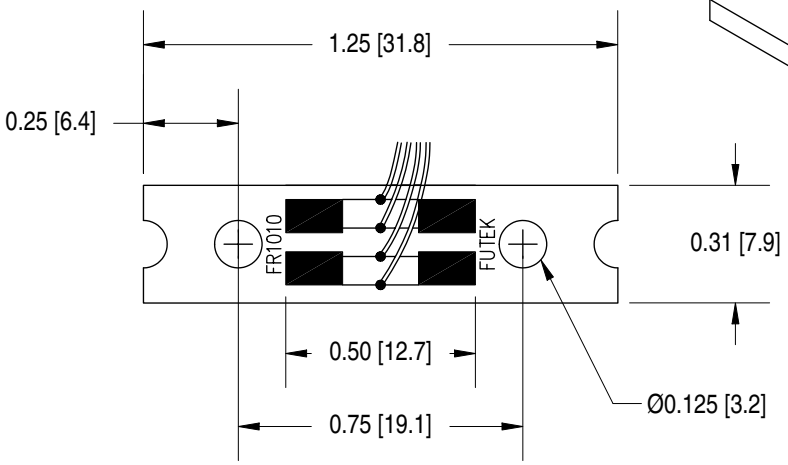

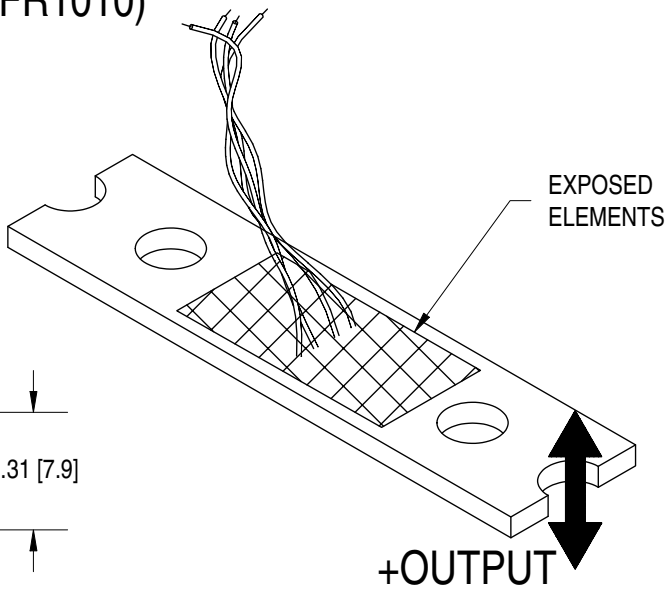

STK#	CAPACITY lb	CAPACITY N	T
FSH01451	1	4.5	0.01 [0.28]
FSH01452	2	8.9	0.015 [0.39]
FSH01453	5	22.2	0.025 [0.64]
FSH01454	10	44.5	0.031 [0.76]
FSH01455	20	89	0.048 [1.22]
FSH01456	40	178	0.06 [1.52]

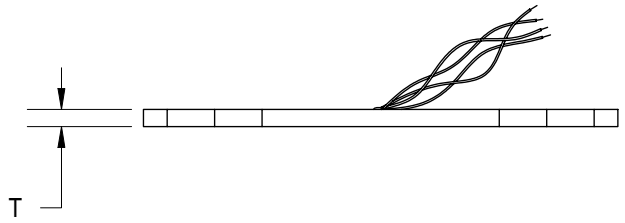

AVAILABLE MOUNTING KIT FOR MORE INFORMATION SEE DWG FI1114

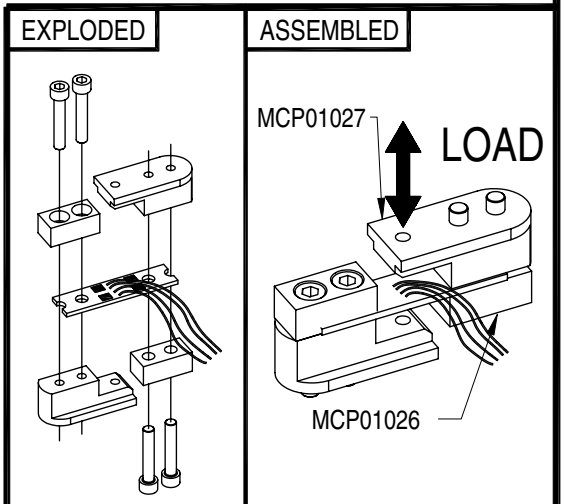

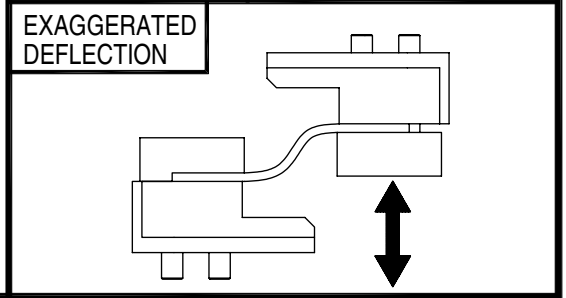

SPECIFICATIONS:

RATED OUTPUT	*2 mV/V nom.*
SAFE OVERLOAD	*150% of R.O.*
ZERO BALANCE	*±5% of R.O.*
EXCITATION (VDC OR VAC)	*18 MAX*
BRIDGE RESISTANCE	*1200±300 Ω*
INSULATION RESISTANCE	*1000 M ohms @ 50 VDC*
COMBINED ERROR	*±0.25% of R.O. } ACTUAL LEVEL OF ACCURACY*
NONREPEATABILITY	*±0.05% of R.O. } DEPENDS ON CLAMPING METHOD.*
TEMP. SHIFT ZERO	*±0.02% of R.O./°F [0.036% of R.O./°C]*
TEMP. SHIFT SPAN	*±0.02% of LOAD/°F [0.036% of LOAD/°C]*
COMPENSATED TEMP.	*60 to 160°F [15 to 72°C]*
OPERATING TEMP.	*-60 to 200°F [-50 to 93°C]*
MATERIAL	*300 SERIES S.S.*
WEIGHT	*0.35 oz [10 g]*
DEFLECTION	*0.004 to 0.010 [0.10 to 0.25] nom.*

CABLE: #29 AWG, 4 Conductor, Spiral Shielded Silicone Cable 1 ft [0.3 m] Long

FUTEK
ADVANCED SENSOR TECHNOLOGY, INC.

10 THOMAS
IRVINE, CA 92618 USA
1-800-23-FUTEK (38835)

INTERNET:
http://www.futek.com

E Matériau sélectionné pour la peau

Saint-Gobain Korel® K30-15 Soft Micro-cellular Polyurethane Foam

Categories: Polymer; Thermoplastic; Polyurethane, TP; Thermoset; Polyurethane, TS; Thermoset Polyurethane Foam, Unreinforced

Material Notes:

Description: The Korel® series micro-cellular polyurethane foams are offered in a broad range of properties, making them ideal for a variety of gasketing and energy absorption needs. Korel® microcellular foams are categorized by degree of deflection force. By varying the modulus and density, Saint Gobain Performance Plastics has developed this series of materials that meets the demands of design engineers today. All Korel fians are available with an aggressive acrylic adhesive on one side to facilitate placement. **Korel K30** foams are soft, conformable, low deflection, urethane foams offering excellent compression set resistance and low out-gassing that exceeds fogging requirements. K30 is ideal for open/close applications.

FEATURES/BENEFITS:

- Excellent compression set resistance
- Highly resilient (will not collapse)
- Dissipates stresses
- Resistant to moisture and most chemicals
- Conformable and flexible even in extreme environmental conditions
- Easy to achieve intricate die-cut parts
- Aggressive acrylic adhesive (optional) facilitates assembly
- Available cast on to polyester film for stability and low deformation

Typical Applications: Cellular telephones, electrical enclosures, electronic gasketing, vibration damping, cushioning, acoustical control, bumpers, instrument panels, spacers.
Specification Notes: Passes Fogging Test SAE-J 1756, 3 hrs. at 212℉ (100℃). All data based on a 0.25 inch test sample.(Available in multiple thicknesses.)
Information provided by Saint Gobain Performance Products.

Thermal Properties	Metric	English	Comments
Thermal Conductivity	0.0865 W/m-K	0.600 BTU-in/hr-ft²-℉	ASTM E1530
Maximum Service Temperature, Air	70.0 ℃	158 ℉	Constant use
	121 ℃	250 ℉	Intermittent

Descriptive Properties	
Standard Color	Black

Some of the values displayed above may have been converted from their original units and/or rounded in order to display the information in a consistant format. Users requiring more precise data for scientific or engineering calculations can click on the property value to see the original value as well as raw conversions to equivalent units. We advise that you only use the original value or one of its raw conversions in your calculations to minimize rounding error. We also ask that you refer to MatWeb's disclaimer and terms of use regarding this information. Click here to view all the property values for this datasheet as they were originally entered into MatWeb.

F Valeurs de e_a et de e_b en fonction du ratio $F(\rho)$

F(ρ)	e_a	e_b
0.0000	0.0507	0.0507
0.0466	0.0523	0.0491
0.1075	0.0545	0.0472
0.1973	0.0582	0.0445
0.2545	0.0607	0.0429
0.3204	0.0639	0.0411
0.3954	0.0681	0.0391
0.4795	0.0738	0.0369
0.5342	0.0780	0.0354
0.5721	0.0814	0.0344
0.6113	0.0853	0.0333
0.6521	0.0899	0.0322
0.6716	0.0925	0.0316
0.6920	0.0953	0.0310
0.7126	0.0984	0.0304
0.7332	0.1020	0.0298
0.7538	0.1060	0.0291
0.7579	0.1070	0.0290
0.7620	0.1070	0.0289
0.7661	0.1080	0.0287
0.7702	0.1090	0.0286
0.7743	0.1100	0.0285
0.7784	0.1110	0.0283
0.7825	0.1120	0.0282
0.7866	0.1130	0.0280
0.7907	0.1140	0.0279
0.7948	0.1150	0.0278
0.7988	0.1160	0.0276
0.8029	0.1170	0.0275
0.8069	0.1180	0.0273
0.8110	0.1190	0.0272
0.8150	0.1200	0.0270
0.8190	0.1210	0.0269
0.8230	0.1230	0.0267
0.8270	0.1240	0.0266

F(ρ)	e_a	e_b
0.8270	0.1240	0.0266
0.8310	0.1250	0.0264
0.8350	0.1260	0.0263
0.8389	0.1280	0.0261
0.8428	0.1290	0.0260
0.8468	0.1300	0.0258
0.8507	0.1320	0.0256
0.8545	0.1330	0.0255
0.8584	0.1350	0.0253
0.8623	0.1370	0.0251
0.8661	0.1380	0.0250
0.8699	0.1400	0.0248
0.8737	0.1420	0.0246
0.8774	0.1440	0.0245
0.8811	0.1460	0.0243
0.8849	0.1480	0.0241
0.8885	0.1500	0.0239
0.8922	0.1520	0.0237
0.8958	0.1540	0.0236
0.8994	0.1560	0.0234
0.9030	0.1590	0.0232
0.9065	0.1610	0.0230
0.9100	0.1640	0.0228
0.9134	0.1660	0.0225
0.9269	0.1790	0.0218
0.9428	0.1980	0.0206
0.9458	0.2020	0.0204
0.9488	0.2070	0.0202
0.9517	0.2120	0.0199
0.9574	0.2230	0.0194
0.9705	0.2580	0.0180
0.9818	0.3120	0.0163
0.9909	0.4080	0.0143
0.9973	0.6480	0.0113
1.0000	∞	0.0000

Combining Haptic Sensing with Safe Interaction

Martin Battaglia, Laurent Blanchet, Abderrahmane Kheddar, Suuji Kajita and Kazuhito Yokoi

***Abstract*— We propose a solution which combines haptic sensing with safe interaction, at low cost. Contact locations are made through a flexible sheet of tactile binary switch matrix. This sheet covers the surface of a rigid bumper module assembled to the robot's basic link through a distributed pressure sensing units. Combination of location and force provides the haptic sensing module. The haptic system is covered with a flexible outer material which role is to absorb contact impacts and to cast local surface profile on which the robot can take support. This overall system allows having a combined haptic sensing with safe and robust physical interaction with both the environment and the human using active compliance. We discuss the benefit of such a simple and modular concept and present how to design the cover material. A simple prototype is realized and experienced.**

I. INTRODUCTION

Haptic sensing and safe interaction with the environment and humans are two challenging issues in robotics in general, and in humanoid robots in particular. These issues are crucial and even interrelated when humanoid robots are allowed to take contact supports with entire body on any part of the environment. This example highlights the importance for the robot to know where contacts occurred on its body and what is the total force wrench applied on each of its links, it also bring to light the importance to have robust contact formation for a stable whole-body motions support; see a thorough discussion of this example in [1].

Recent researches are tackling the problem of haptic sensing through bio-mimetic approaches (artificial skin). These approaches are interesting and challenging; several admirable technologies and designs have been proposed to build an artificial sensing skin. However, we distinguish between haptic sensing that is used for whole-body motions, interaction and closed-loop task realization, from that haptic sensing used for robot perception and acquisition of haptic knowledge or precise dexterous manipulation. There are also considerable works in achieving human-robot safety collocated physical human-robot interaction through various techniques that can be gathered in two main categories: active, passive or hybrid compliance. Several very sophisticated design and prototypes have been recently demonstrated with very impressive results.

Our work aims at designing a combined haptic sensing and active safety interaction system which can cover the entire body of the robot for whole body motion and at low cost. It will be used for detecting, locating and absorbing safely the contacts and the collisions of both the (humanoid) robot and its surrounding. Such a combined system is very useful for a humanoid robot operating in a changing environment where objects and possibly human beings are moving. The total humanoid's cover surface is important enough for parameters such as cost, weight, and thickness to be critical.

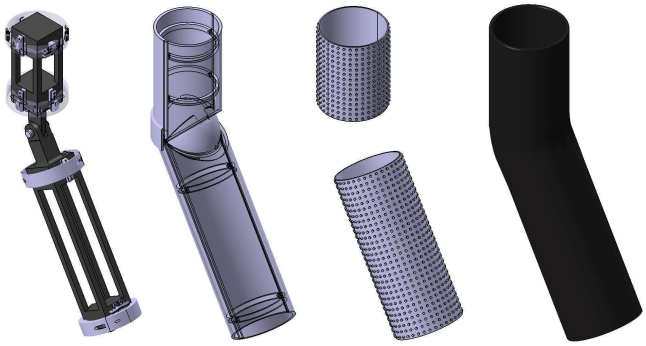

Fig. 1. Exploded view of the whole design for an arm, from left to right: the robot links (dark) and the distributed pressure sensors (gray rings), the bumper, the contact location tactile binary switches, the compliant cover.

Our approach is driven by practical viewpoints, as will be seen later on, some researches have taken more or less a similar path considering similar constraints. We simply went a bit further in our investigations to see how a combined whole-body haptic and safe interaction can be tackled with a pragmatic way for real usage and applicability. We consider any link of the robot to be made of two main parts: (i) the proper robot link, and (ii) our system; the later consists in four parts, Fig. 1: (ii) a simple shape bumper surrounding the robot's link and attached to it through (i) distributed pressure sensor units; (iii) a contact location sensor, being a thin sheet of matrix tactile binary switches (in its simplest form), and which covers entirely the bumper: its role is to provide contact locations (contact surfaces and their barycenter), and (iv) a compliant material (foam) covering the tactile sheet which role is to well cast the contacting surface and to absorb chocks at the contact spots.

The first part of the paper discusses the overall concept; the second part focuses on a computation tool allowing to determine the characteristics of the compliant outer cover; the third part presents a preliminary proof-of-concept.

This work was supported in part by the EC FP6 Contract No 034002 www.robot-at-cwe.eu

M. Battaglia and A. Kheddar are with the Centre National de la Recherche Scientifique, CNRS-UM2 LIRMM, Montpellier, France, and with the CNRS-AIST JRL, UMI3218/CRT, Tsukuba, Japan. battaglia,kheddar@lirmm.fr

L. Blanchet is with ENS Cachan, France, and with the CNRS-AIST JRL UMI3218/CRT, Tsukuba, Japan. blanchet@crans.org

S. Kajita and K. Yokoi are with the Humanoid Research Group of the Intelligent Systems Research Institute of the National Institute of Advanced Industrial Science and Technology, Tsukuba, Japan. s.kajita,kazuhito.yokoi@aist.go.jp

II. Proposed Solution

Our solution combines whole-body haptic sensing and safety interaction function. The requirements that drove our approach are summarized as follows:

- coverage of wide areas of robot's links with minimum signal processing, latencies, and data flow on the robot's network or bus;
- usage of a flexible outer cover to absorb impacts due to desired or not desired contacts, and to locally cast surface profile; it can also be used for aesthetics;
- location, on the robot, of contact areas and measurement of force wrenches per link;
- modular, quickly demountable, interchangeable with an easily maintenance and life cycle;
- not costly, light and with reasonable thickness

We devised a modular system which allows combining simple technologies in a multilevel design described in Fig. 1. Starting from a bare robot's link, we attach to it a rigid simple shaped cover (bumper) through distributed pressure units which deformation measures the resultant force wrench acting on the link. Distributing pressure units on the link is preferable to having a single location of force measure e.g. using a commercial 6dof force sensor. Yet, an optimal distribution and location is to be found for each link by restricting the number of the pressure units (if possible to 6 or less). This part will be published in another paper.

The bumper is covered by a flexible tactile sensing sheet, see Fig. 1. Its role is to sample the contact spots on each link. That is, where contacts occur and, for each contact, an estimate of its area and barycenter. Our choice would have been to use flexible keyboards technology, since it is simple, mature and cheap enough. But the switches are mechanical whereas capacitive switches may have superior advantages. Other options are possible. In [2], a sensitive skin is developed on the basis of single sided electrode units covered by a conductive rubber with a resistivity which depends on the applied pressure. Their matrix tactile system needs one wire per taxel and could basically be used in our case. In [3] a multi-contact detection sensor sheet based on resistive measurement consists in two conductive plates each in a discrete combination of parallel conductive bands are separated by a pressure sensitive material that acts as an electrical insulator under no load but conduct electricity when pressure is applied. The material is chosen for its electric characteristics and the thickness being a result of the fabrication process. If bended in a low curvature, it could be damaged. The work by [4] uses the same physical principle for measuring the pressure distribution, but with a grid architecture, what reduces the number of wires to one per line and one per column. Using the same kind of conductive rubber, the system shown in [5] goes further in the reduction of the wires number by using electrical impedance tomography that allows measurement only on the borders of the skin to obtain pressure distribution and can basically be used in our design. Since we consider pressure sensor units to have the resultant force wrench on each link, quantifying the pressure information is not necessary in our case. That is why we can certainly make previous technologies simpler or thinner, or make use of binary on/off switches. It is what we did for the proof-of-concept, with putting a diode after each switch to avoid ghosting effect. There are obviously several additional technologies which we did not mention not only because of space but also because they are not mature enough for use. We are however investigating capacitive switches.

At this stage we have the choice between designing the tactile sensor with (i) thick resistive or capacitive foam so that the tactile sensor could also absorb impacts, or (ii) a thin tactile sensor and a separate additional flexible cover to absorb impacts. We decided to win the second choice for many reasons. Among which, the freedom to design the sensor with optimal resolution using best of resistive and capacitive material layers, avoid using stretchable technologies for the tactile sensor since they compose the surface of the link, protect the sensor by its inner location possibility i.e. between the bumper and the flexible cover, design the cover with esthetic shapes, etc.

Once the tactile sensor technology is decided, it is covered by a flexible material which role is to absorb impacts during the necessary time to detect it and react to it (active compliance), and also to cast well the surface to build robust whole-body motion supporting contacts. This part is very important and need to be carefully designed. Authors in [6] considered criteria borrowed from human injury data and tested impact with different materials. Recent researches make use of data from crash-tests in automobile industry [7]. But to our best knowledge, the model for mechanical characteristics and the thickness determination of the cover has not been thoroughly studied. This paper focuses on computation of the thickness for a given material or on characterizing the material both under constraints related to the issue of haptic sensing and safe interaction. We also study the influence of the flexible cover's thickness and the resolution on the sensitivity of the tactile sheet.

III. Flexible cover's characteristics

We based our characterization of the cover on the excellent review of the impact problem performed by Stronge [8]. We build a method for computing the material properties of a cover given a set of well defined constraints. First, we define a set of relations linking several parameters involved in the characterization of the cover's material. Only after, we explain the algorithm which makes use of these relations in an interactive design process.

Consider two bodies B and B' for which the following parameters can be defined. The effective modulus: $E_* = \left[\left(1-\nu_B^2\right)E_B^{-1} + \left(1-\nu_{B'}^2\right)E_{B'}^{-1}\right]^{-1}$ where E_i is the Young's modulus (Pa) and ν_i the Poisson's ratio of the body i; the effective radius: $R_* = \left[R_B^{-1} + R_{B'}^{-1}\right]^{-1}$ where R_i is the local radius of curvature of the body i (m) at the contact point; the effective mass: $m_* = \left[m_B^{-1} + m_{B'}^{-1}\right]^{-1}$ where m_i is the contact projected mass of the body i.

The collided body, B', is the obstacle and its mechanical characteristics are considered known (worst case setting). We

want here to cover the colliding robot body B with a flexible material, whose goal is to absorb the impact during the time needed to detect and to react (computation of the active compliance), which is a given time constraint τ (seconds).

A. Impact model

In chapter 6 of [8], Stronge established the impact model for free colliding spherical bodies; we followed similar computation steps for establishing an impact model that would apply for the system represented in Fig. 2. It is a 1dof robotic motorized link, covered by elastic foam and for which we establish the impact model in the worst case, i.e. when it hits a rigid, unmovable obstacle like a wall corner.

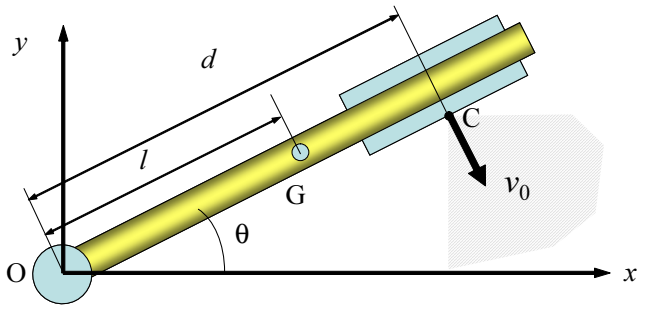

Fig. 2. Illustration of the prototype case study.

In this simple case study, C is the contact point, G the center of mass, O the origin, d the distance between the contact point and the origin, l the distance between the center of mass and the origin, and θ the joint angle of the arm. The dynamic model for the arm is:

$$J\ddot{\theta} + Mgl\sin\theta = u - dF \tag{1}$$

where $J = \frac{m_B}{12}(3R_B^2 + d^2) + m_B l^2$ is the moment of inertia, u the motor torque, and $F = K_s\delta^{3/2}$ the contact force, with $K_s = \frac{4}{3}E_* R_*^{1/2}$ [8]. The relations $\ddot{\theta} = \frac{\ddot{\delta}}{d}$ and $\theta - \theta_0 = \frac{\delta}{d}$ lead to:

$$\frac{J}{d}\ddot{\delta} + Mgl\sin\left(\theta_0 + \frac{\delta}{d}\right) = u - dK_s\delta^{3/2} \tag{2}$$

where θ_0 the angle of the arm at the contact. Considering that $\ddot{\delta} = \dot{\delta}\frac{d\dot{\delta}}{d\delta}$ and the initial conditions $\dot{\delta}(0) = -v_0$ and $\delta(0) = 0$, the integration of the previous equation gives:

$$\frac{J}{2d}(\dot{\delta}^2 - v_0^2) - Mgld\cos\left(\theta_0 + \frac{\delta}{d}\right) = u\delta - \frac{2dK_s}{5}\delta^{5/2} \tag{3}$$

When the compression phase ends, at $t = t_c$, the normal relative velocity vanishes, so $\dot{\delta} = 0$, $\delta = \delta_c$, and as $\delta << d$, $\cos\left(\theta_0 + \frac{\delta}{d}\right) \approx \cos\theta_0$. The eq. (3) gives us the expression of the compression time:

$$t_c = \int_0^{\delta_c}\left(v_0^2 + \frac{2d^2}{J}Mgl\cos\theta_0 + \frac{2du\delta}{J} - \frac{4K_s d^2}{5J}\delta^{5/2}\right)^{-1/2} d\delta \tag{4}$$

and becomes:

$$\frac{J}{2d}v_0^2 + Mgld\cos(\theta_0) = -u\delta_c + \frac{2dK_s}{5}\delta_c^{5/2} \tag{5}$$

None of these two equations has an analytical solution, so we can not find an analytical expression of E_* in function of t_c as done in the Stronge's example.

B. Yield aspect

Whatever material we choose, we will forbid to reach the plastic domain during compression so that the impact does not become rigid. This second part is in quasi-static and the results depend of the material and the geometry, not of the mechanical structure and the dynamics of the robot. The effective modulus gives us the ratio $\frac{E_B}{1-\nu_B^2}$, what we use to choose a material and so to obtain Y_B, the yield stress of the body B (Pa). The transition contact pressure between the elastic and the plastic domains is $p_Y = \nu_Y Y_B$. It occurs for the body B at the indentation limit for elastic deformation δ_Y obtained from:

$$\frac{p_Y}{Y_B} = \nu_Y = \frac{4E_*}{3\pi Y_B}\sqrt{\frac{\delta_Y}{R_*}} \tag{6}$$

where the ratio ν_Y depends on the geometry of the contact (for example, for a contact between two spheres: $\nu_Y = 1.1$ and between a cylinder and a plane: $\nu_Y = 1.5$). This leads to the non-dimensional indentation $\frac{\delta_Y}{R_*}$ required to initiate yield, a material property:

$$\frac{\delta_Y}{R_*} = \left(\frac{3\pi}{4}\right)^2\left(\frac{\nu_Y Y_B}{E_*}\right)^2 \tag{7}$$

We do not make use of eq. (7) explicitly, it is checked at each step of the design process to ensure that the indentation do not reach the yield limit.

C. Skin thickness for energy absorbing

Let U_r be the material resilience which defines the energy that the material can elastically absorb per unit of volume. We know that a sphere/cylinder contact (our case study), is elliptic and can be expressed, according to Hertz's contact theory as $S_c = 1.3\pi\left(\frac{FR_*}{E_*}\right)^{2/3}$. Finite element simulations show that volume absorbing the energy can be approximated by a cylinder with a surface 4 times bigger in both dimensions than the contact area, i.e. $16S_c$, the thickness e being its height.

Considering the energy absorption rate linear leads to the energy to be absorbed by the skin: $E_n = E_k \cdot (t_0/t_c)$, with t_c the time that would have been required if the skin had to absorb all the impact as defined before. W is the work done by the contact effort and we state that all of the energy is transmitted to the material (again, worst case scenario) so $W = E_n$. Stronge's work [8] gives us: $\frac{W}{E_* R_*^3} = \frac{8}{15}\left(\frac{\delta}{R_*}\right)^{5/2}$ thus the effort : $F = \left(\left(\frac{8}{15}\right)^2 E_k^3 E_*^2 R_*\right)^{1/5}$.

The resilience U_r is given by $U_r = \frac{Y_B 2}{2E_B}$. Considering that $U_r e 16 S_c = E_n$, and that $E_k = \frac{1}{2}mv_0^2$, we have:

$$e = \frac{m^{3/5}\cdot v_0^{6/5}\cdot(t_0/t_c)}{84\cdot U_r\cdot\left(R_*^2 E_*^{-1}\right)^{6/15}} \tag{8}$$

D. Sensitivity of the sensor

We will use a sensor build as a square matrix of switch. As this sensor does discrete contact detection, it is important to estimate the sensitivity of the sensor, i.e. the necessary contact force to be detected, considering the thickness and the resolution of the matrix, i.e. distance between two switches.

We based our study on [9] (Chapt. 3). We consider a semi-infinite, homogeneous, linear elastic, incompressible (i.e. with a Poisson ratio of 0.5) material, on which a normal punctual force F is applied. We define σ_z the stress in the normal direction of a given point. This model states:

$$F = \frac{2\sigma_z \pi (x^2+y^2+z^2)^{5/2}}{3z^3} \tag{9}$$

where (x,y,z) are the coordinates of a point relative to the contact point, the contact point being the origin. In the worst case, i.e. the contact point being equidistant of each switch, we set the point on the center of the switch. There, we have $\sigma_z = \frac{F_s}{S}$, where F_s is the necessary force to press the switch until the electrical contact and S the surface of the contact between the switch and the cover, $x^2+y^2 = \frac{d^2}{2}$, d being the resolution of the matrix and $z = e$, e being the thickness of the skin. We obtain:

$$F = \frac{2F_s \pi (\frac{d^2}{2}+e^2)^{5/2}}{3Se^3} \tag{10}$$

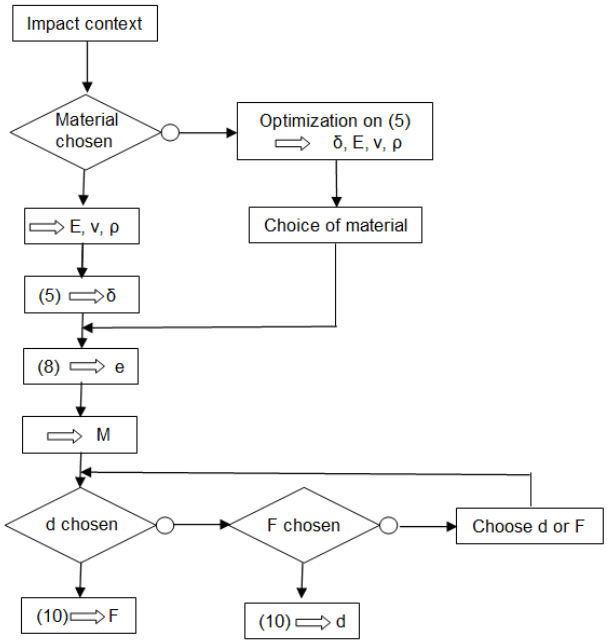

Fig. 3. Schematic of the algorithm.

E. Algorithm for material, thickness and other parameters determination

Now, considering a given situation of impact (geometrical, inertial and impact parameters known) and a given sensor technology (F_s and S known), we determine the unknown parameters for designing the cover material, E_B being the Young modulus, e the thickness and ρ the density of the skin, and F the minimal detectable force by the sensor and d the resolution of the sensor. We can have some constrains on parameters set by external factors, for instance $d < d_{\max}$ and $F < F_{\max}$, or $e < e_{\max}$. Those constraints must be checked at every step of the algorithm. If not, we have to reconsider the constraints, or to make different choices, namely a different material.

IV. Prototype

We devised a 1dof motorized arm as a proof-of-concept to perform experiments prior to a first prototype. It is made of a stainless tube attached to the force sensor which in turns is linked to a DC motor. We also realized the tactile matrix, and the polyurethane foam plate on it, see Fig. 4.

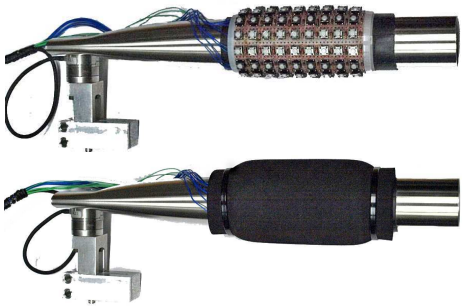

Fig. 4. Assembled prototype.

A. Design

We took Elastomeric foams as the cover material. This material can extend more than 100% in a classical traction test and remain in the elastic domain. Sensors' screenings and control computation latencies sum to $t_0 \approx 6$ms (we set it to $\tau = 8$ms). The characteristics of arm are $m_B = 0.6$kg, $R_B = 38$mm, $l = 150$mm and $d = 200$mm. The initial speed is $v_0 = 0.4\text{m.s}^{-1}$ and the contact angle is $\theta_0 = 0$rad. The other constants are $R_{B'} = 38$mm and $g = 9.81\text{m.s}^{-2}$.

Our algorithm gives the following solution: $E_B = 3.6510^5$Pa and $\delta_c = 3.2$mm. We found a material fitting this characteristic thanks to the Matweb database: the micro-cellular polyurethane foam (Young modulus is $E = 3.45\ 10^5$Pa, yield stress is $Y_B = 8.4110^5$Pa). We changed some values of our device to increase safety $m = 2$kg and $v_0 = 1.5\text{m.s}^{-1}$, and use the characteristics of the chosen material in eq. (8); we obtained the following results: $U_r = 4791\text{J.m}^{-3}$ and $e = 7.90$mm. We found micro-cellular polyurethane foam in 5mm and 10mm thick plate, so we used both as a good approximation of the results of the model, depending of the degree of safety.

In case of sudden contact (switch on), we stop the ongoing motion and reverse it up to the contact detection. We also made an active compliance using the force sensor. We decided of a limit the torque to 3Nm for couple, this value being the rated range of our sensor, which corresponds to

15N for the contact effort, the distance between the sensor and the contact being 20cm.

B. Tactile sheet prototype

We designed a simple matrix of commercial on/off mechanical small switches combined with a force sensor mounted between the link and the actuator; it has 1cm resolution spacing. The keyboard pattern leads to a reduced number of wires that allows a direct connection to the I/O card we used for data processing. In case of an extension of the matrix, i.e. an increase of the number of wires, multiplexing is necessary.

Main computations are done at the same time; to optimize the contact detection time we used a FPGA chip, programmed with VHDL language. These chip and language are particularly designed for task parallelization. The two main tasks are (i) to identify contact zones, i.e. to gather adjacent pressed switches in the same contact set, and (ii) to compute the area and the barycenter of each contact zone.

C. Experiment

We conducted experiments to assess the principle of the system, i.e. detecting the contact and the subsequent in the motion's direction. We also evaluated the efforts resulting from the contact. The experimentation consists in moving the arm into an obstacle. A human arm is used as a sudden obstacle; once detected, the controller reverses the motion, until the contact is resolved, and finally slowing down until its stops.

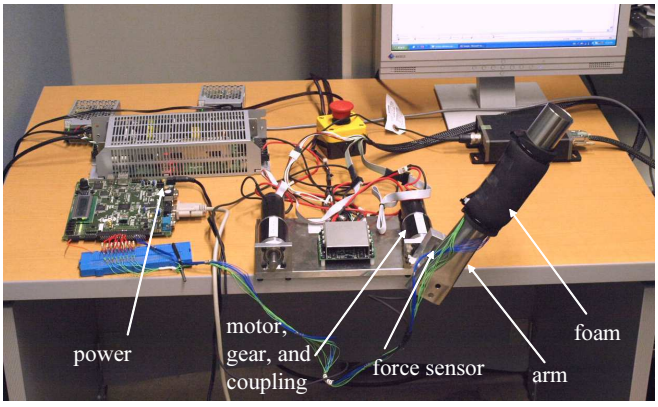

Fig. 5. Experimental set-up.

We led the experiment with two thicknesses of the flexible foam cover, 5mm and 10mm, the Figs. 6 and 7 show the results of the experiment for the 5mm thick cover. The influence of the thickness is studied further. The Fig. 6 represents the evolution of the angular speed of the arm, and the Fig 7 the evolution of the torque between the arm and the motor.

The Fig. 6 illustrates that the system achieves the previously described behavior. The Fig. 7 shows that the contact is not instantaneously detected, but that the torque, i.e. the contact force, has to reach a certain value for the electrical contact in a switch to be realized.

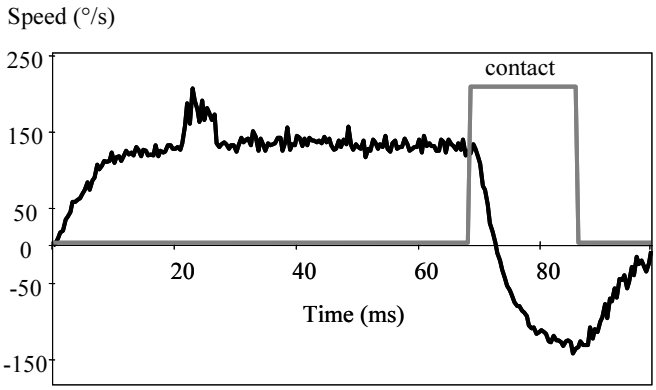

Fig. 6. Measurement of the speed during the experiment.

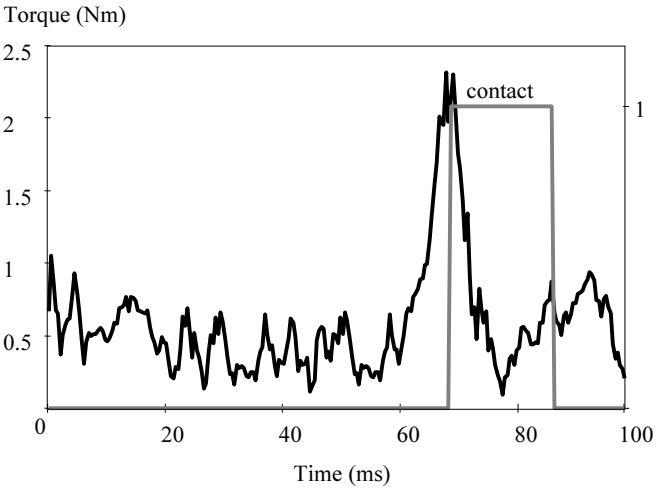

Fig. 7. Measurement of the torque during the experiment.

The measured values are 2.3Nm for the torque, so 12N for the contact force, the distance between the contact point and the torque sensor being 20cm.

We noted that if the speed starts decreasing as soon as the contact is detected, it stays positive for around 5ms, when the torque immediately decreases, what could be surprising considering that the compression continues as long as the speed is positive. The explanation of this phenomenon is that the measured torque is between the motor and the arm, so when the contact is detected, the reference for the motor immediately changes and the motor tries to go back, when the mechanical inertia of the arm maintains the speed positive for a short time. Indeed the mechanical inertia is higher than the electrical one. It is not really significant in this case, but that point must be kept in mind and taken into account for the next developments of the system.

For our the tactile system we devised, the characteristics of a unit switch are $F_m = 1\text{N}$ and $S = 12.6\ 10^{-6}\text{m}^2$, $0 < d < 0.005\sqrt{2}\text{m}$ and $z = 0.005\text{m}$, which leads the graphics in Fig. 8.

As we can see on Fig. 8 and from the equation (9), the necessary force to initiate detection grows as a six degree polynomial to $F_c = 65\text{N}$ for $d = 0.005\sqrt{2}$, i.e. at the

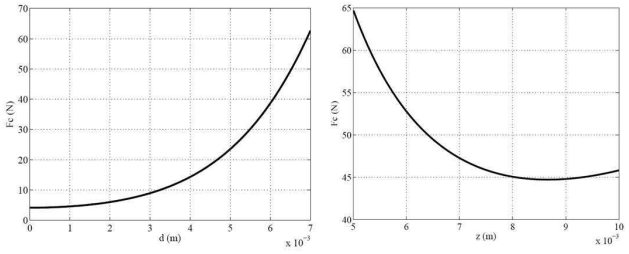

Fig. 8. Contact force in function of the distance for $z = 5$mm and of the thickness for $d = 5\sqrt{2}$mm.

maximum possible distance from a switch.

If we know the force by measurement, as in our experiment described above, we can easily invert this model to evaluate the distance between the contact point and the switch. In our example, we measured $F_c = 12$N, so the value of the distance is $d = 0.0036$m.

We can also see the influence of thickness on the necessary contact force, at the farthest point of any switch, for $d = 0.005\sqrt{2}$m. It shows that in this particular case, the minimal contact force is $F_c = 45$N, equivalent to a 8.5Nm torque at the central point of the force sensor. Considering that the security limit for our force sensor is 3Nm, which stops the system when reached, the maximum contact force acceptable is therefore 15N. It is not possible for it to be detected at $d = 0.005\sqrt{2}$m, as the Fig. 8 showed. From the Fig. 8 and from the equation (9), in the case of a 5mm cover, we find that the maximum distance is $d = 4.2$mm. It means a definition of 5.9mm, as d is the half-diagonal of the square made by the 4 switches around the contact point.

Here this sensitivity study suggests to us to reconsider our initial choice of definition, to ensure contact detection considering the physical limits of the prototype.

D. Linear elastic hypothesis

We run compression tests on our material which led to the results shown on the Fig. 9. This figure shows that the material has an elastic linear behavior up to at least 30N for both thicknesses. The correlation coefficient being superior to 0.99. Therefore, since the maximum measured force in our experiment is 12N, the material remains in the elastic linear domain and the hypothesis made for all computations hold.

V. Conclusion

We proposed a simple design to combine at low cost haptic sensing with safe interaction and robust contact formation through outer cover compliance. This system appears to be modular enough to be envisaged as a potential solution to embed haptic sensing and compliance to humanoid robots. We devised a simple one degree of freedom prototype which assesses the feasibility of the idea. We also proposed a method to design the cover and proved it detect collisions and react according to the strategy envisaged for the control. the haptic function combines a flexible sheet of on/off switches

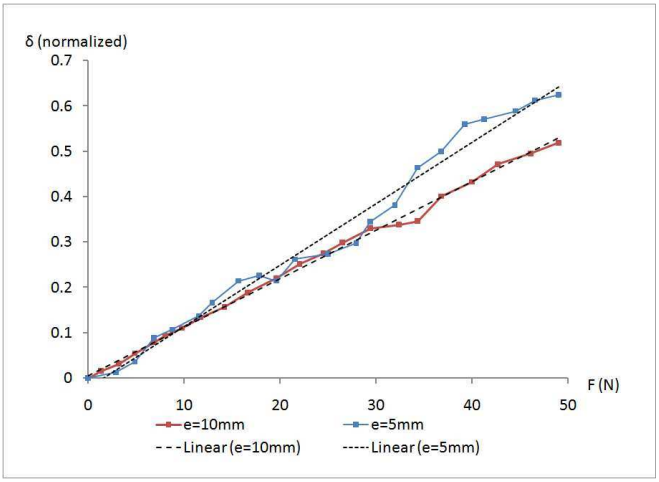

Fig. 9. Deformation in function of the force for both 5mm and 10mm thicknesses.

with a force sensor that could be embedded with a bumper mechanism. It proves the validity of this principle of a tactile soft cover to introduce a safety against collision for the robot and its environment. Furthermore, the sensitivity study gives us valuable information about the possible thickness and definition, considering a limit contact force and a certain kind of switch.

The next step of this work will be to design, on the basis of this principle, a better sensor extensible to a larger area and able to be installed on a real robot, and to solve the problem of sensing at the area of the joint's of the robot.

References

[1] A. Kheddar and A. Escande, "Challenges in contact-support planning for acyclic motion of humanoids and androids," in *39th International Symposium on Robotics*, Seoul, Korea, October 15-17 2008, pp. 740–745.

[2] D. Goeger, K. Weiss, C. Burghart, and H. Woern, "Sensitive skin for a humanoid robot," in *Human-Centered Robotic Systems*, Munich, Germany, October 6-7 2006, pp. 115–120.

[3] V. Duchaine, N. Lauzier, M. Baril, M.-A. Lacasse, and C. Gosselin, "A flexible robot skin for safe physical human robot interaction," in *IEEE International Conference on Robotics and Automation*, Kobe, Japan, May 12-17 2009, pp. 3676–3681.

[4] X. Lamy, F. Colledani, F. Geffard, Y. Measson, and G. Morel, "Robotic skin structure and performances for industrial robot comanipulation," in *IEEE/ASME International Conference on Advanced Intelligent Mechatronics*, Singapore, July 14-17 2009, pp. 427–432.

[5] A. Nagakubo, H. Alirezaei, and Y. Kuniyoshi, "A deformable and deformation sensitive tactile distribution sensor," in *IEEE International Conference on Robotics and Biomimetics*, Sanya, China, December 15-18 2007, pp. 1301–1308.

[6] T. Sugaiwa, H. Iwata, and S. Sugano, "Shock absorbing skin design for human-symbiotic robot at the worst case collision," in *IEEE-RAS International Conference on Humanoid Robots*, Daejeon, Korea, December 1-3 2008, pp. 481–486.

[7] S. Haddadin, A. Albu-Schaeffer, M. Frommberger, J. Rossmann, and G. Hirzinger, "The DLR crash report: towards a standard crash-testing protocol for robot safety - part I and II," in *IEEE International Conference on Robotics and Automation*, Kobe, Japan, May 12-17 2009, pp. 272–287.

[8] W. J. Stronge, *Impact mechanics*. Cambridge University Press, 2000.

[9] K. L. Johnson, *Contact mechanics*. Cambridge University Press, 1985.